Attitude and Orbit Control of a Spinning Solar Sail by the Vibrational Input on the Sail Membrane

By Yuki TAKAO[1)]

[1)]*Department of Aeronautics and Astronautics, The University of Tokyo, Tokyo, Japan*

(Received June 21st, 2017)

An attitude and orbit control method for a spinning solar sail utilizing the active shape control of the sail membrane is investigated. Spinning type membrane space structures easily deform because they have no supporting structures. This may lead to the unexpected change of the effect of solar radiation pressure (SRP) on the membranes. Since the SRP is a dominant factor of the dynamics of membrane space structures, especially for solar sails, the knowledge of the deformation is vital to them. However, it is almost impossible to precisely predict and design the actual deformation of the membrane before deployment. In this study, an active shape control method for membrane space structures is proposed, and is applied to the attitude and orbit control of a spinning solar sail.

Key Words: Solar Sail, Solar Radiation Pressure, Shape Control, Vibration Mode

Nomenclature

t	:	time
x, y, z	:	Cartesian coordinate
r, θ, z	:	cylindrical coordinate
$\boldsymbol{r}$	:	position vector
M	:	mass
w	:	out-of-plane deformation
Ω	:	spin rate (angular velocity)
r_a	:	inner radius
r_b	:	outer radius
h	:	thickness
ρ	:	density
ν'	:	Poison's ratio
σ	:	tensile stress
R, Θ	:	mode function
q	:	modal coordinate
ω	:	natural frequency
ν	:	circumferential order of vibration
n	:	radial order of vibration
L	:	Standard length
l	:	arm length
I	:	moment of inertia
$\boldsymbol{n}$	:	normal vector
$\boldsymbol{s}$	:	sun vector
ψ, ϕ	:	in-plane and out-of-plane sun angle
F, f	:	force
T, τ	:	torque
P	:	momentum flux
S	:	area
C_{spe}	:	specular reflectivity
C_{dif}	:	diffuse reflectivity
C_{abs}	:	absorptivity
B_f	:	Lambertian coefficient
A, B, a, b	:	constants of integration
p, λ, N, Q, γ	:	other constants
Σ	:	coordinate system
$\delta_{x,y}$	:	Dirac's delta

Superscripts

$\hat{}$	:	dimensionless value
$\bar{}$	:	complex conjugate
$\tilde{}$	:	forced response
I	:	inertial frame
O	:	orbit-fixed frame
SF	:	spin-free-fixed frame

Subscripts

r, θ, z	:	direction in cylindrical coordinate
ν, μ	:	circumferential order of vibration
n, m	:	radial order of vibration
0	:	input by forced vibration
SRP	:	solar radiation pressure
M	:	membrane
B	:	main body

1. Introduction

Recently, the use of flexible membrane structures is gathering attention in the space field. They allows carrying lightweight structures with large area to space, and are expected to be widely used in the future. One of the membrane structures is solar sail. Solar sail is a spacecraft which is driven by solar radiation pressure (SRP), so that it can be propelled basically without any propellant. Fig. 1 shows the small solar sail demonstrator IKAROS launched in 2010 by Japan Aerospace Exploration Agency.[1)]

Membrane structures including solar sails can be classified roughly into two types depending on the deployment method of the membrane. One is mast-extension type, which deploys its membrane by use of inflatable mast structures. Another is spinning type, which deploys by centrifugal force. Since spinning type ones do not require any supporting structure, they are preferable in terms of system weight. In case of solar sail, spinning type is still more preferable because the propulsion performance is better when the ratio of area to mass is larger. However, spinning type membrane structures easily deform due to the lack of supporting structures. This may cause the unex-

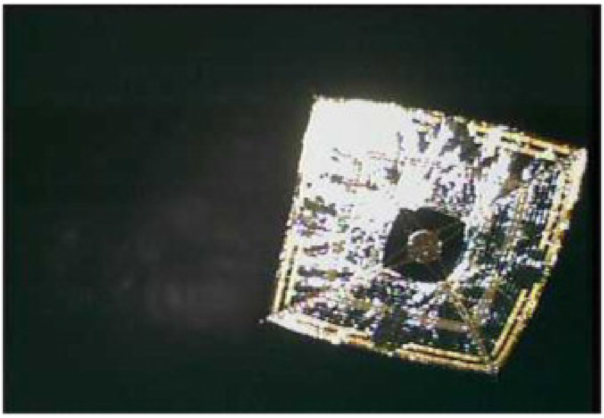

Fig. 1.: Spinning solar sail demonstrator IKAROS with its 14m × 14m large sail membrane.[1] Photographed by a deployable camera on the orbit.

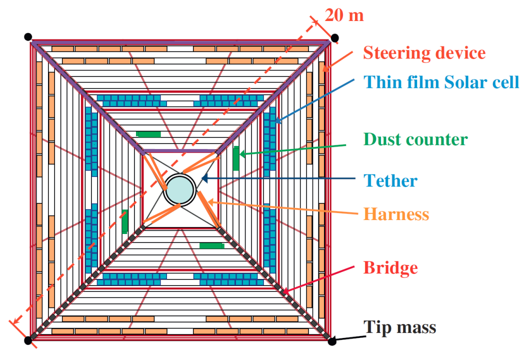

Fig. 2.: Configuration of IKAROS.[1]

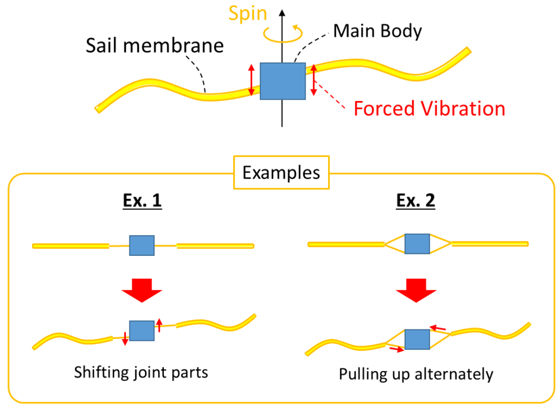

Fig. 3.: Concept of the shape control method for spinning membrane structures, and examples with tethers.

pected change of the SRP on its membrane, which largely affects the attitude motion (and orbital motion in case of solar sails) of the spacecraft.[2]

Reflectivity control device (RCD)[3] is one solution to deal with the problem. It can change optical property of the surface electrically to control the SRP on it. Hence, switching multiple RCDs distributed on the membrane can cause the unbalance of the solar radiation force to generate the attitude control torque. However, RCDs have a problem of space environmental effects. Performance of RCDs is also affected by the deformation of the membrane. Therefore, knowledge of deformation of the membrane is vital not only to solar sailing, but to achieving general spinning type membrane space structures. Nevertheless, deformation of the flexible membrane structures is complex, unpredictable, and few studies have dealt with the active control of it.

This paper proposes an active shape control method for a spinning type membrane space structures by the vibrational input. In concrete, the method aims to actively vibrate the membrane by use of mechanical actuators to induce a certain vibration mode on it. In particular, we show that the shape control method works even if the vibrational input is limited to one-dimensional one.

This method allows launching various missions with membrane structures. For example, the method makes it possible to control the thrust and torque that originate in the SRP. This can be applied to the attitude and orbit control of a solar sail. In another example, thin-film devices that are attached on the membrane can change their orientation; e.g. performance of thin-film solar cells can be enhanced by changing their orientation to the sun, even if the main body of the spacecraft has some pointing requirements. In the same way, not only can the reflection direction of RCDs be controlled, combination of torque control via shape control and the one via RCDs can realize the novel control of attitude motion.

The dynamics of membrane space structures is complex, in which structure, attitude, and orbit are coupled. The method proposed in this study allows controlling this dynamics, which has an infinite degree of freedom, only by a one-dimensional vibrational input.

In the following sections, the concrete way of the shape control is proposed first. Next, vibration mode of spinning membrane structures is derived analytically assuming a simple model. Then, a numerical analysis is conducted to show the validity and applicability of the analytical solution to general membrane structures. Finally, an optimal attitude and orbit control of a spinning solar sail is performed as an example of the application of the developed shape control method.

2. Shape Control of Membrane Structures

2.1. Shape control method

The flexible membrane structures are easily deformed with vibrations. The vibrations are theoretically described by a superposition of multiple vibration modes. When a certain periodic input is given on the membrane, and its frequency is enough close to the natural frequency of the structure, the corresponding vibration mode is then induced on the membrane. When the input wave consists of multiple waves superposed, the membrane can form various complex shapes.

The periodic input can be, for example, given as a forced vibration by use of mechanical actuators. In case of IKAROS, the sail membrane and the main body of the spacecraft are connected via tethers (Fig. 2). This paper proposes to drive the tethers for the shape control. Two ways are possible to give the vibrational input by use of tethers (Fig. 3). One is to shift the joint parts between the tethers and the main body up and down (Ex. 1). Another is to pull up tethers alternately which are attached at the top and bottom part, respectively, of the main body (Ex. 2).

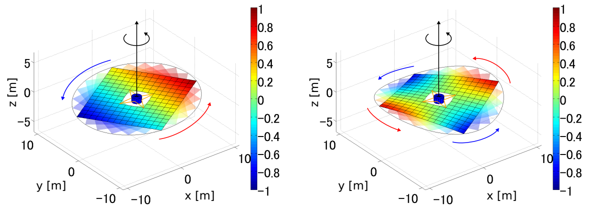

(a) Example 1. (b) Example 2.

Fig. 4.: Examples of static waves in the inertial frame. Contour shows the normalized displacement for z direction.

2.2. Static waveform in the inertial frame

The effect of the vibration on the SRP is usually time-averaged because it is a periodic motion. However, the waveform of the vibration can be completely static in the inertial frame when the frequency of the vibrational input is synchronized with the spin rate of the system. The reason is that the vibrational input (i.e. the motion of tethers) draws a fixed trajectory in the inertial frame when the above-mentioned condition is satisfied. Therefore, the effect of the SRP can be constantly changed by use of static waves. Figure 4 shows the examples of the static wave. The detailed condition to induce static waves is mentioned in the next section.

3. Analytical Vibration Mode Analysis of Spinning Membrane Structures

Vibrations of spinning membrane structures is analytically derived in this section. Here, a uniform circular membrane is assumed for the simplicity. Vibrations of membrane structures consist of in-plane and out-of-plane ones, and they can be treated independently in the linear region.[4] Hence, the out-of-plane vibration, which is the target of the shape control, is modeled. Response to the vibrational input is also analyzed. Finally the conditions to form a static wave is discussed on the basis of the analytical solution.

3.1. Vibration mode analysis

3.1.1. Derivation of the mode function

Assume a spinning, uniform, circular membrane structure as shown in Fig. 5. The deformation of the membrane is described in the rotating cylindrical coordinate $r-\theta-z$, whose origin is at the center of the membrane. The spin rate of the system is constant. The force for z direction exerted on the microelement $dM = \rho hrdrd\theta$ is described as follow.

$$F_z = \left\{\frac{\partial}{\partial r}\left(\sigma_r\frac{\partial w}{\partial r}r\right) + \frac{\partial}{\partial \theta}\left(\sigma_\theta\frac{\partial w}{r\partial \theta}\right)\right\}hrdrd\theta \tag{1}$$

Hence, equation of motion is written as follow.

$$\begin{aligned} &\ddot{w}dM = F_z \\ \Leftrightarrow\ &\rho r\frac{\partial^2 w}{\partial t^2} = \frac{\partial}{\partial r}\left(\sigma_r\frac{\partial w}{\partial r}r\right) + \frac{\partial}{\partial \theta}\left(\sigma_\theta\frac{\partial w}{r\partial \theta}\right) \end{aligned} \tag{2}$$

Considering a plane stress state of a spinning circular membrane, tensile stress for radial and circumferential direction is, respectively, derived as follows when $r_a = 0$.

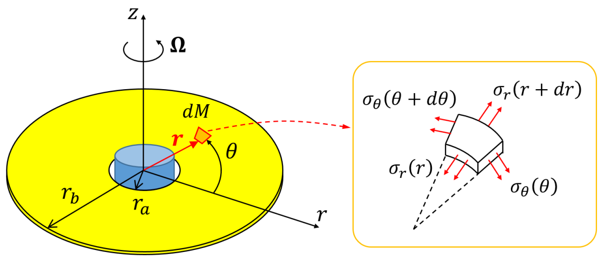

Fig. 5.: Analysis model of vibrations of spinning membrane structures.

$$\begin{aligned} \sigma_r &= \frac{3+\nu'}{8}\rho\Omega^2 r_b^2\left(1-\frac{r^2}{r_b^2}\right) \\ \sigma_\theta &= \frac{3+\nu'}{8}\rho\Omega^2 r_b^2\left(1-\frac{1+3\nu'}{3+\nu'}\frac{r^2}{r_b^2}\right) \end{aligned} \tag{3}$$

Here, the following solution is assumed considering the separation of variables.

$$w(r,\theta,t) = R(r)\Theta(\theta)q(t) \tag{4}$$

Substituting Eq. (4) into Eq. (2), the following equations are obtained.

$$\frac{d^2q}{dt^2} + \omega^2 q = 0 \tag{5}$$

$$\frac{d^2\Theta}{d\theta^2} + \nu^2\Theta = 0 \tag{6}$$

$$r\frac{d}{dr}\left(\sigma_r\frac{dR}{dr}r\right) + (\rho\omega^2 r^2 - \nu^2\sigma_\theta)R = 0 \tag{7}$$

ω and ν appear as the constants of separation of variables. The boundary conditions are given as follows.

$$\Theta(\theta) = \Theta(\theta+2\pi) \tag{8}$$

$$R(r_b) < \infty \tag{9}$$

Equations (8) and (9) mean, respectively, the continuity for circumferential direction, and the free edge boundary condition. Since the solution of $\Theta(\theta)$ can be described sinusoidally, Eq. (8) gives the following condition.

$$\nu = 0,\ 1,\ 2,\ 3,\ \cdots \tag{10}$$

Substituting Eq. (3) into Eq. (7), differential equation of $R(r)$ is described as follow.

$$\hat{r}\frac{d}{d\hat{r}}\left\{\hat{r}(1-\hat{r}^2)\frac{dR}{d\hat{r}}\right\} + (\lambda^2\hat{r}^2 - \nu^2)R = 0 \tag{11}$$

where

$$\hat{r} = \frac{r}{r_b} \tag{12}$$

$$\lambda^2 = \frac{8}{3+\nu'}\left(\frac{\omega}{\Omega}\right)^2 + \frac{1+3\nu'}{3+\nu'} \geq 0 \tag{13}$$

Assume the following solution for Eq. (11), which starts from the p-th order.

$$R(\hat{r}) = \hat{r}^p\sum_{m=0}^{\infty}a_m\hat{r}^m \tag{14}$$

Substituting Eq. (14) into Eq. (11), and evaluating the coefficient of $\hat{r}^p$, p is derived as

$$p = \pm\nu \tag{15}$$

Since the solution of $R(\hat{r})$ diverges at $\hat{r} = 0$ when $p = -\nu$, which conflicts with Eq. (9), only the case of $p = \nu$ is enough to describe the actual deformation. Therefore, the following recurrence formula of a_m is derived by substituting Eq. (14) into Eq. (11) under $p = \nu$.

$$\begin{aligned} a_m &= \frac{(m+\nu-2)(m+\nu)-\lambda^2}{m(m+2\nu)} a_{m-2} \\ a_0 &\neq 0 \\ a_{-1} &= 0 \end{aligned} \tag{16}$$

The following condition is required to satisfy Eq. (9).

$$\begin{gathered} \exists n \in O, \lambda^2 = (n+\nu-1)(n+\nu+1), n \geq 1 \\ O = \{x \in \mathbb{Z} | x \text{ is odd}\} \end{gathered} \tag{17}$$

This is because a_m is zero in the $n+1$ th or higher order, and the infinite series (14) becomes a polynomial of degree $n-1$ when Eq. (17) holds. Otherwise the solution diverges at $\hat{r} = 1$. Let n denote the order of vibration for radial direction. Natural frequency is then expressed as the following equation, by substituting Eq. (17) into Eq. (13).

$$\omega_{\nu,n} = \Omega\sqrt{\frac{3+\nu'}{8}(\nu+n-1)(\nu+n+1) - \frac{1+3\nu'}{8}\nu^2} \tag{18}$$

Subscript means that the natural frequency depends both on circumferential and radial order of vibration. Eq. (16) can be rewritten as follow, by substituting Eq. (17).

$$a_m = \frac{(m-n-1)(m+n+2\nu-1)}{m(m+2\nu)} a_{m-2} \tag{19}$$

Therefore, the general term of a_m can be expressed as follow.

$$\begin{aligned} a_{2k} &= (-1)^{k+\frac{n-1}{2}} \binom{\frac{n-1}{2}}{\frac{n-1}{2}-k} \binom{k+\nu+\frac{n-1}{2}}{k+\nu} \\ a_{2k+1} &= 0 \end{aligned} \tag{20}$$

Thus, the general solution of the radial mode function is described as follow.

$$R_{\nu,n}(\hat{r}) = \sum_{k=0}^{\frac{n-1}{2}} (-1)^{k+\frac{n-1}{2}} \binom{\frac{n-1}{2}}{\frac{n-1}{2}-k} \binom{k+\nu+\frac{n-1}{2}}{k+\nu} \hat{r}^{\nu+2k} \tag{21}$$

Finally, the general solution of the vibration of a spinning circular membrane is expressed as follow.

$$\begin{aligned} w(r,\theta,t) &= \sum_{\nu}\sum_{n} R_{\nu,n}\left(\frac{r}{r_b}\right)\Theta_\nu(\theta) q_{\nu,n}(t) \\ &= \sum_{\nu}\sum_{n} R_{\nu,n}\left(\frac{r}{r_b}\right)\left\{A_{\nu,n}e^{i(\nu\theta+\omega_{\nu,n}t+a)} + B_{\nu,n}e^{i(\nu\theta-\omega_{\nu,n}t+b)}\right\} \end{aligned} \tag{22}$$

Figure 6 shows the examples of analytical vibration modes expressed by Eq. (22).

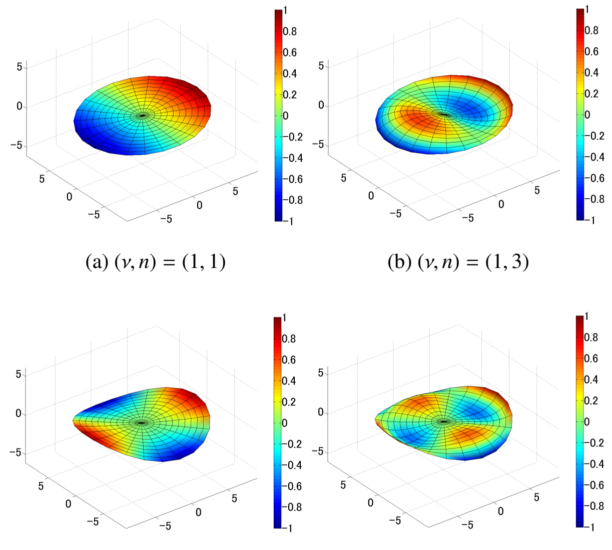

(a) $(\nu, n) = (1, 1)$ (b) $(\nu, n) = (1, 3)$

(c) $(\nu, n) = (2, 1)$ (d) $(\nu, n) = (2, 3)$

Fig. 6.: Vibration modes of a spinning circular membrane.

3.1.2. Orthogonality of the mode function

Equation (11) in the (ν, n)-th order can be written as

$$\left(\lambda_{\nu,n}^2\hat{r} - \frac{\nu^2}{\hat{r}}\right)R_{\nu,n} = -\frac{d}{d\hat{r}}\left\{\hat{r}(1-\hat{r}^2)\frac{dR_{\nu,n}}{d\hat{r}}\right\} \tag{23}$$

where

$$\lambda_{\nu,n}^2 = (\nu+n-1)(\nu+n+1) \tag{24}$$

from Eq. (17). By integrating the multiple of Eq. (23) and $R_{\nu,m}$, the following equation is obtained.

$$\int_0^1 \left(\lambda_{\nu,n}^2\hat{r} - \frac{\nu^2}{\hat{r}}\right)R_{\nu,m}R_{\nu,n}d\hat{r} = \int_0^1 \hat{r}(1-\hat{r}^2)\frac{dR_{\nu,m}}{d\hat{r}}\frac{dR_{\nu,n}}{d\hat{r}}d\hat{r} \tag{25}$$

In the same way, the following equation is obtained about the (ν, m)-th order.

$$\int_0^1 \left(\lambda_{\nu,m}^2\hat{r} - \frac{\nu^2}{\hat{r}}\right)R_{\nu,n}R_{\nu,m}d\hat{r} = \int_0^1 \hat{r}(1-\hat{r}^2)\frac{dR_{\nu,n}}{d\hat{r}}\frac{dR_{\nu,m}}{d\hat{r}}d\hat{r} \tag{26}$$

Calculating Eq. (25) $-$ Eq. (26), the following equation is derived.

$$(\lambda_{\nu,n}^2 - \lambda_{\nu,m}^2)\int_0^1 \hat{r}R_{\nu,m}R_{\nu,n}d\hat{r} = 0 \tag{27}$$

Since $\lambda_{\nu,m}^2 \neq \lambda_{\nu,n}^2$ when $m \neq n$, the following equation holds.

$$\int_0^1 \hat{r}R_{\nu,m}R_{\nu,n}d\hat{r} = 0 \quad (m \neq n) \tag{28}$$

Thus, orthogonality of the radial function about its order n is confirmed. In addition to the case of circumferential mode function, the orthogonality is described by following equations.

$$\begin{gathered} \int_0^1 \hat{r}R_{\nu,m}R_{\nu,n}d\hat{r} = N_{\nu,n}\delta_{m,n} \\ \int_0^{2\pi} \Theta_\mu\bar{\Theta}_\nu d\theta = 2\pi\delta_{\mu,\nu} \end{gathered} \tag{29}$$

3.2. Forced response analysis

When the vibrational input is given to the membrane by tethers, the forced displacement at $r = r_a$ can be expressed as follow.

$$w(r_a, \theta, t) = w_0(\theta, t) = A_0 e^{i(\nu_0\theta+\omega_0 t+a_0)} + B_0 e^{i(\nu_0\theta-\omega_0 t+b_0)} \quad (30)$$

When the deformation of the membrane is described as $w(r, \theta, t) = \tilde{w}(r, \theta, t)+w_0(\theta, t)$, equation of motion (2) is rewritten as follow.

$$\rho r \frac{\partial^2 \tilde{w}}{\partial t^2} = \frac{\partial}{\partial r}\left(\sigma_r \frac{\partial \tilde{w}}{\partial r} r\right) + \frac{\partial}{\partial \theta}\left(\sigma_\theta \frac{\partial \tilde{w}}{r\partial \theta}\right) + F_0 \quad (31)$$

where

$$F_0 = -\rho r \frac{\partial^2 w_0}{\partial t^2} + \frac{\partial}{\partial \theta}\left(\sigma_\theta \frac{\partial w_0}{r\partial \theta}\right) \quad (32)$$

F_0 denote a kind of inertial force which appears when considering the deformation via $\tilde{w}$. From Eq. (30), F_0 can be rewritten as follow.

$$F_0 = \left(\rho r \omega_0^2 - \frac{\sigma_\theta}{r}\nu_0^2\right) w_0 \quad (33)$$

Assuming that the vibration mode here is also described by the same mode function as in Eq. (22), $\tilde{w}$ can be described as follow.

$$\tilde{w}(r, \theta, t) = \sum_\nu \sum_n R_{\nu,n}\left(\frac{r}{r_b}\right)\Theta_\nu(\theta)\tilde{q}_{\nu,n}(t) \quad (34)$$

From Eqs. (6), (7), (31) and (34), the following equation is obtained.

$$\sum_\nu \sum_n R_{\nu,n}\Theta_\nu\left(\frac{d^2\tilde{q}_{\nu,n}}{dt^2} + \omega_{\nu,n}^2\tilde{q}_{\nu,n}\right) = \frac{F_0}{\rho r} \quad (35)$$

Applying the orthogonality of mode functions described in Eq. (29) to Eq. (35), the following equation is derived.

$$\begin{aligned}\frac{d^2\tilde{q}_{\nu,n}}{dt^2} + \omega_{\nu,n}^2\tilde{q}_{\nu,n} &= \frac{1}{2\pi N_{\nu,n}}\iint \frac{\hat{r}R_{\nu,n}\bar{\Theta}_\nu F_0}{\rho r} dr d\theta \\ &= \frac{1}{2\pi\rho r_b N_{\nu,n}}\iint R_{\nu,n}\bar{\Theta}_\nu F_0 dr d\theta\end{aligned} \quad (36)$$

Substituting Eq. (33) into Eq. (36), the differential equation of the modal coordinate $\tilde{q}_{\nu,n}$ is derived as follow.

$$\frac{d^2\tilde{q}_{\nu,n}}{dt^2} + \omega_{\nu,n}^2\tilde{q}_{\nu,n} = Q_{\nu,n}\delta_{\nu_0,\nu}\left\{A_0 e^{i(\omega_0 t+a_0)} + B_0 e^{i(-\omega_0 t+b_0)}\right\} \quad (37)$$

where

$$Q_{\nu,n} = \frac{1}{\rho r_b N_{\nu,n}}\int\left(\rho r\omega_0^2 - \frac{\sigma_\theta}{r}\nu_0^2\right)R_{\nu,n} dr \quad (38)$$

Particular solution of Eq. (37) is

$$\tilde{q}_{\nu,n} = \frac{Q_{\nu,n}\delta_{\nu_0\nu}}{\omega_{\nu,n}^2 - \omega_0^2}\left\{A_0 e^{i(\omega_0 t+a_0)} + B_0 e^{i(-\omega_0 t+b_0)}\right\} \quad (39)$$

Therefore, the response to the vibrational input is expressed by the following equation.

$$\begin{aligned}&\tilde{w}(r, \theta, t) \\ &= \sum_n \frac{Q_{\nu_0,n}}{\omega_{\nu_0,n}^2 - \omega_0^2} R_{\nu_0,n}\left(\frac{r}{r_b}\right)\left\{A_0 e^{i(\nu_0\theta+\omega_0 t+a_0)} + B_0 e^{i(\nu_0\theta-\omega_0 t+b_0)}\right\}\end{aligned} \quad (40)$$

As can be seen from Eq. (40), only ν_0-th order mode appears for circumferential direction while the resonance magnification for radial direction is determined by the input frequency ω_0 and the natural frequency $\omega_{\nu_0,n}$.

3.3. How to induce the static wave

From Eq. (40), the vibration is expressed by the superposition of progressive wave and regressive wave for the circumferential direction.

$$\begin{aligned}\text{progressive wave :} \quad & B_0 e^{i\left\{\nu_0(\theta - \frac{\omega_0}{\nu_0}t)+b_0\right\}} \\ \text{regressive wave :} \quad & A_0 e^{i\left\{\nu_0(\theta + \frac{\omega_0}{\nu_0}t)+a_0\right\}}\end{aligned}$$

Their velocity for θ direction is ω_0/ν_0 and $-\omega_0/\nu_0$ respectively in the rotating frame. Considering that the angular velocity of the rotating frame is Ω, the velocity of the waves in the inertial frame is expressed as $\Omega + \omega_0/\nu_0$ and $\Omega - \omega_0/\nu_0$ respectively. When the following conditions are satisfied, the velocity of the regressive wave is zero and hence the induced waveform is static in the inertial frame.

$$\begin{aligned}&B_0 = 0 \\ &\Omega - \omega_0/\nu_0 \;\Leftrightarrow\; \omega_0 = \nu_0\Omega\end{aligned} \quad (41)$$

Equation (41) means that the input frequency must be synchronized with the spin rate to induce the static deformation, as described in section **2.2.**. In addition, the vibrational input must be given so that the progressive wave for θ direction does not occur. The vibrational input which induces a static wave is, from the conditions, expressed as follow.

$$w_0(\theta, t) = A_0 e^{i(\nu_0\theta+\nu_0\Omega t+a_0)} \quad (42)$$

The corresponding static waveform of the membrane in the inertial frame is then derived as follow.

$$\tilde{w}^I(r, \theta) = \sum_n \frac{A_0 Q_{\nu_0,n}}{\omega_{\nu_0,n}^2 - (\nu_0\Omega)^2} R_{\nu_0,n}\left(\frac{r}{r_b}\right) e^{i(\nu_0\theta+a_0)} \quad (43)$$

The static wave is essentially expressed as the superposition of vibrations of every radial order, but actually, only domestic order vibrations appear depending on the resonance magnification. Following equations show the representative shape of the static wave, in the low-frequency region from $\nu_0 = 1$ to 4.

$$\begin{aligned}w_1^I(r, \theta) &= A_1\cos(\theta + a_1) + \tilde{A}_1 R_{1,1}\cos(\theta + a_1) \\ w_2^I(r, \theta) &= A_2\cos(2\theta + a_2) + \tilde{A}_2 R_{2,1}\cos(2\theta + a_2) \\ w_3^I(r, \theta) &= A_3\cos(3\theta + a_3) + \tilde{A}_3 R_{3,3}\cos(3\theta + a_3) \\ w_4^I(r, \theta) &= A_4\cos(4\theta + a_4) + \tilde{A}_4 R_{4,3}\cos(4\theta + a_4)\end{aligned} \quad (44)$$

In the following, they are called "ν_0-th order static wave". Number of subscripts corresponds to the order of vibration.

4. Feasibility Evaluation

In section **3.**, vibration mode and forced response of a spinning membrane structure are analytically derived assuming a simple theoretical model. On the other hand, this assumption is not necessarily available to general membrane structures. For example, IKAROS has a square-shaped sail membrane due to the folding and packing method. The center of the membrane is empty to hold the main body for the same reason. Also, the deformation induced by the proposed method is expected to

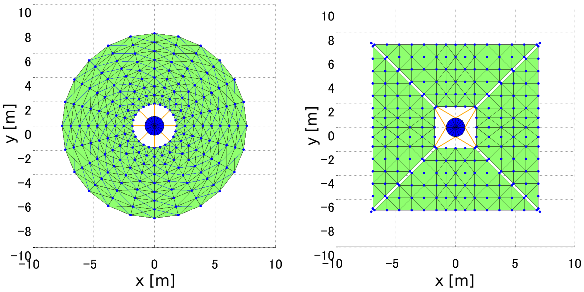

(a) Circular model. (b) Square model.

Fig. 7.: Distribution of particles for the MPM.

Table 1.: Properties of the spacecraft.

All system	Spin rate	1.0	rpm
Main body	Mass	295	kg
	Diameter	1.58	m
	Height	0.845	m
	Moment of inertia around x, y axis	47.71	$kg \cdot m^2$
	Moment of inertia around z axis	66.48	$kg \cdot m^2$
Membrane	Inner radius	1.8	m
	Outer radius	7.6	m
	Young's modulus	3.2	GPa
	Poisson's ratio	0.33	-
	Structural damping coef.	3.9×10^{-5}	s
	Thickness	7.5	μm
	Density	1420	kg/m^3

be large because of oscillation, while the theoretical model assumes an infinitesimal strain theory in the linear region. However, it is known that principal characteristics of vibrations of actual membrane structures tend to be similar to those of simple theoretical model.[5]

In this section, feasibility of the theoretical model against general membrane structures is evaluated by numerical analysis. First, numerical analysis of a circular membrane validates the theoretical model in the non-linear region with $r_a \neq 0$. Next, deformation behavior of square-shaped membrane, which is based on the configuration of IKAROS, is analyzed to be compared with that of the circular membrane. Thus, the effectiveness of applying the developed theoretical model to the general membrane structures is verified.

4.1. Multi-particle model

A method called multi-particle model (MPM)[6] is utilized in the numerical analysis. MPM simulates the thin-film membrane structure by spring-mass system. In this model, a number of particles are distributed across the entire surface of the membrane, and the particles are connected by springs and dampers. Since computational cost of the MPM is rather small than that of finite element method, the MPM is suitable for analyzing the global behavior of the membrane structures. Figure 7 shows the configuration of the MPM used in this study.

Spring constants in the MPM is determined on the basis of the principle of virtual work; so that the elastic energy as the spring-mass system is identical to the strain energy as the continuum. Table 1 shows the properties of the spacecraft used in the analysis. The main body is treated as a cylindrical rigid body. Tethers and bridges are also modeled as springs from their elastic properties. Parameters of the membrane derive from those of IKAROS sail membrane. Inner and outer radius of the circular membrane are determined so that the area of the membrane is identical to that of IKAROS sail.

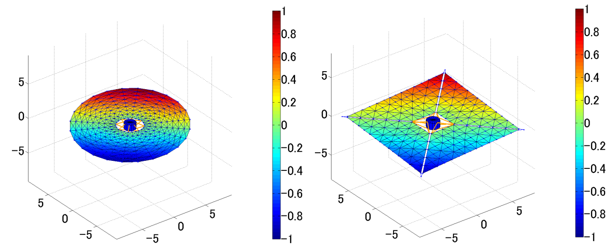

(a) Circular. (b) Square.

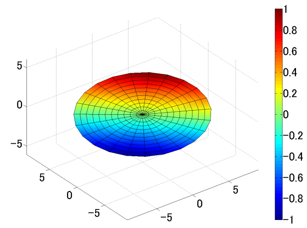

(c) Analytical.

Fig. 8.: $(\nu, n) = (1, 1)$-th mode obtained by the MPM.

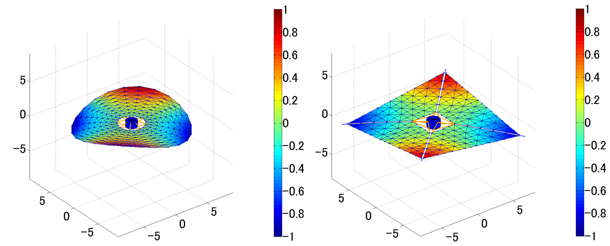

(a) Circular. (b) Square.

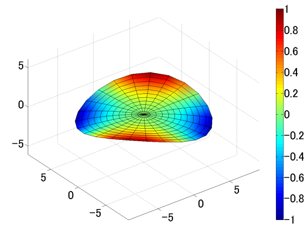

(c) Analytical.

Fig. 9.: $(\nu, n) = (2, 1)$-th mode obtained by the MPM.

4.2. Mode analysis

The membrane is replaced as a spring-mass system by applying the MPM. Vibration mode analysis is thereby available by linearizing equation of motion.[7] Equation of motion of the system can be written in matrix form by setting up linearized simultaneous equations of all particles. Hence, vibration mode and its natural frequency can be calculated by the eigenvalue analysis of the mass matrix and the stiffness matrix.

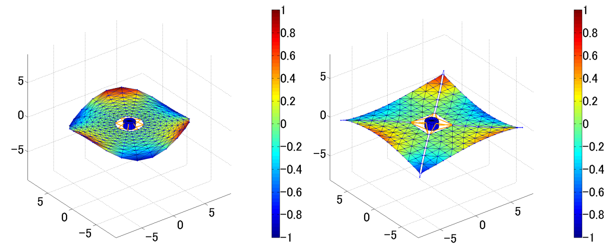

(a) Circular. (b) Square.

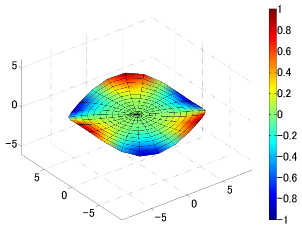

(c) Analytical.

Fig. 10.: $(\nu, n) = (3, 1)$-th mode obtained by the MPM.

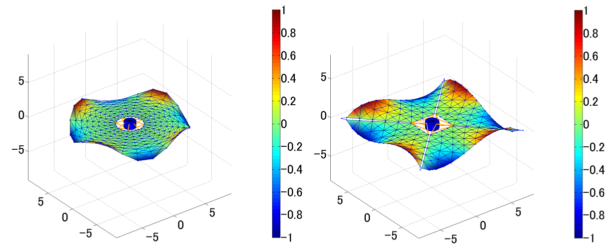

(a) Circular. (b) Square.

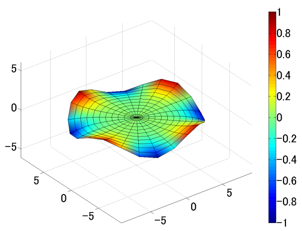

(c) Analytical.

Fig. 11.: $(\nu, n) = (4, 1)$-th mode obtained by the MPM.

Figures 8 through 11 show the vibration modes obtained by the MPM analysis, and their comparison with the analytical solutions. As can be seen from the figures, the numerical analysis result corresponds to the analytical solution in every order. Figure 12 shows the natural frequency of each vibration mode. The figure confirms that the natural frequency of the MPM also shows a similar trend with that of the analytical solution, even though the error between them gets larger in proportion to the order of vibration. As a result, the deformation behavior of both circular and square membrane is expected to be well described by the theoretical model.

4.3. Evaluation of shape control accuracy

Accuracy of the proposed shape control method is evaluated by the numerical simulation with the MPM. The vibrational input is given via tethers to induce the static wave, on the basis of Eq. (42). Tethers are vibrated using pulling-up method de-

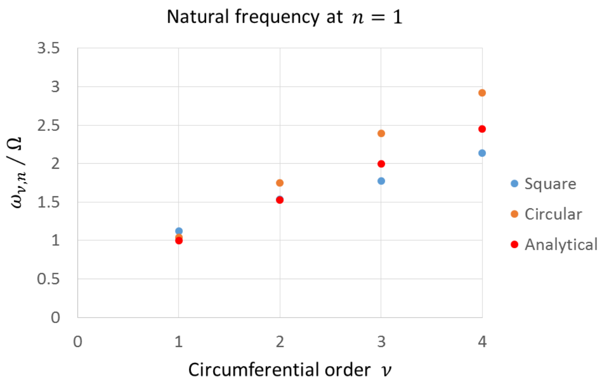

Fig. 12.: Natural frequency of each vibration mode obtained by the MPM. Normalized by the spin rate.

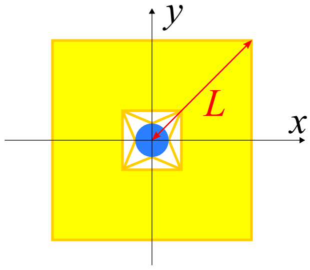

Fig. 13.: Standard length of the square membrane.

scribed in Ex. 2, Fig. 3. The reason for the selection is that the method can give the forced displacement directly at the inner edge of the membrane $r = r_a$. The membrane is completely flat at the initial state ($t = 0$ sec), and the motion is calculated by the numerical integration of equations of motion of the particles.

The target deformations to induce in this simulation are the 1st and 2nd ones, both for the circular and square membrane. The expected deformations to be induced on the circular membrane are written as follows from Eq. (44).

$$
\begin{aligned}
w_1^I(r,\theta) &= A_1 \cos(\theta + a_1) + \tilde{A}_1 \left(\frac{r}{r_a}\right) \cos(\theta + a_1) \\
w_2^I(r,\theta) &= A_2 \cos(2\theta + a_2) + \tilde{A}_2 \left(\frac{r}{r_a}\right)^2 \cos(2\theta + a_2)
\end{aligned}
\tag{45}
$$

Figures 14 and 15 show the simulation results against the 1st and 2nd mode input on the circular membrane respectively. Deformation states in the inertial frame at $t = 2000$ sec and $t = 3000$ sec are described as examples for each one. As can be seen from the figures, the waveform of the membrane is almost the same in each case since the tops and bottoms of the waves are in the same locations. In order to evaluate the accuracy of the shape control method against the analytical solution quantitatively, error analysis is conducted by means of least squares method; calculating mean error between displacement of all particles and the expected shape written in Eq. (45). Figure 16 shows the history of mean errors of the circular membrane. The figure confirms that the control error is almost within 20% through time. The possible reasons for the error are

- discretization error of the membrane by the MPM
- transient response because of the small damping effect
- linearization error against the large deformation

Also, the errors of the 2nd mode response is larger than those of the 1st mode one because the shape of the 2nd mode one is more

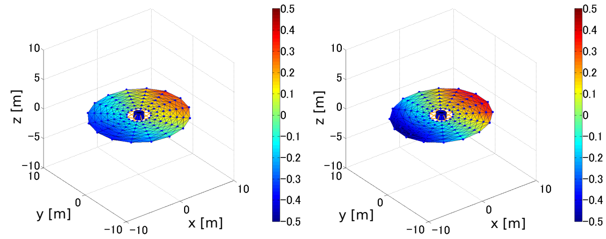

(a) t = 2000 sec. (b) t = 3000 sec.

Fig. 14.: Simulation result of 1st mode static wave (circular).

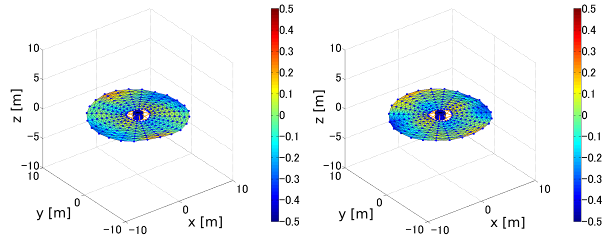

(a) t = 2000 sec. (b) t = 3000 sec.

Fig. 15.: Simulation result of 2nd mode static wave (circular).

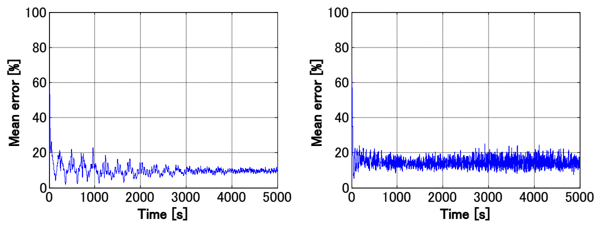

(a) 1st mode static wave. (b) 2nd mode static wave.

Fig. 16.: History of fitting errors of the circular membrane.

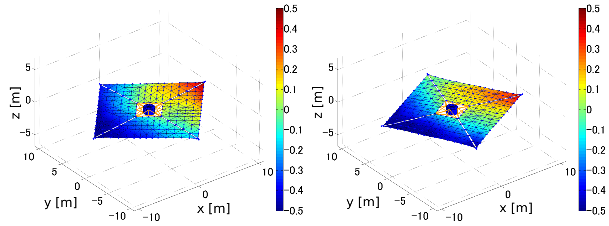

(a) t = 2000 sec. (b) t = 3000 sec.

Fig. 17.: Simulation result of 1st mode static wave (square).

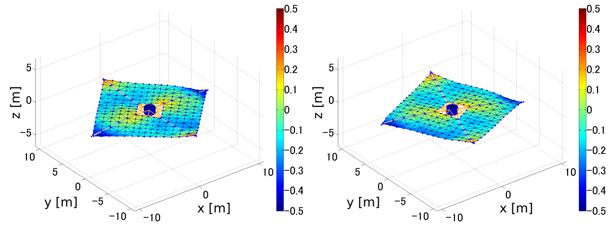

(a) t = 2000 sec. (b) t = 3000 sec.

Fig. 18.: Simulation result of 2nd mode static wave (square).

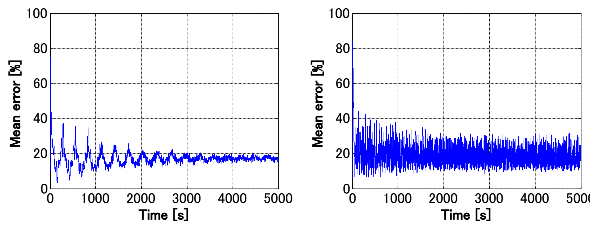

(a) 1st mode static wave. (b) 2nd mode static wave.

Fig. 19.: History of fitting errors of the square membrane.

complex than the 1st mode one. However, the errors converges to a certain value in both cases, and the target vibration mode is induced in the first several tens of seconds.

As for the square membrane, the expected deformations are assumed to be expressed as follows, in which the argument of Eq. (45) is replaced as $\hat{r} = \dfrac{r}{r_b} \rightarrow \dfrac{\sqrt{x^2+y^2}}{L}$.

$$w_1^I(r,\theta) = A_1\cos(\theta + a_1) + \tilde{A}_1\left(\frac{\sqrt{x^2+y^2}}{L}\right)\cos(\theta + a_1)$$
$$w_2^I(r,\theta) = A_2\cos(2\theta + a_2) + \tilde{A}_2\left(\frac{\sqrt{x^2+y^2}}{L}\right)^2\cos(2\theta + a_2) \tag{46}$$

The standard length L is set to be from the center to the outer vertex of the square membrane (Fig. 13). This assumption is considered to be effective in the low-frequency region due to the results of section **4.2.** (Figs. 8 - 11). Figures 17 and 18 show the simulation results of the square membrane. The results confirms that the waveforms of the square membrane is almost static similarly as those of the circular one. Figure 19 shows the history of mean errors of the induced shape. As can be seen, the history shows the similar trends as that of circular membrane even though the errors of the square membrane is relatively larger than those of the circular one. As a result, the shape control method works properly both for circular and square membranes.

5. Application to the Attitude and Orbit Control of a Spinning Solar Sail

In this section, an attitude and orbit control strategy is discussed utilizing the developed shape control method. Thrust vector of a solar sail is determined by the orientation of the sail membrane to the sun. Therefore, attitude of the spacecraft plays a dominant role in its orbital motion. Orbit control of a solar sail is performed by changing its attitude in many studies. The attitude control is performed for example by use of thrusters, or RCDs. This study propose a new method for the attitude and orbit control based on the shape control method with static waves.

5.1. Attitude and orbit control method

As described in the previous sections, the 1st order static wave (Figs. 14 and 15) keeps flat, inclined deformation in the inertial frame. This corresponds to changing the orientation of the sail membrane without changing the attitude (i.e. the angular momentum of the whole system is conserved). The 1st order static wave can, therefore, be applied to the orbit control. As shown in section **4.3.**, time constant of the shape control is quite small compared to that of attitude, and orbital motion. Hence,

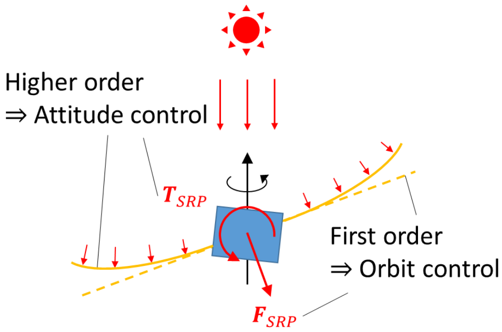

Fig. 20.: Attitude and orbit control strategy.

this orbit control method can not only be performed without any fuel, but achieve faster maneuver of the sail membrane than RCDs.

However, the sail membrane cannot keep its orientation toward a certain point forever because of the SRP disturbance torque; the total angular momentum drifts over the performance of the 1st order static wave. This problem can be solved by the superposition of the 1st and higher order static waves. The super position causes asymmetric deformation of the membrane, which results in additional SRP torque. In summary, thrust is controlled via 1st order static wave, and the attitude disturbance torque is canceled via 2nd order static wave. This leads to the simultaneous control of the attitude and orbital motion. Figure 20 shows the schematic chart of the method.

5.2. Formulation of thrust and torque caused by SRP

As for the derivation of the thrust and torque caused by SRP, orbit-fixed frame Σ^O and spin-free-fixed frame Σ^{SF} are introduced. The orbit-fixed frame moves in accordance with the orbital motion. Its origin is at the center of mass of the spacecraft. z axis is parallel to the sun direction, y axis is perpendicular to the orbital plane, and x axis forms a right-handed system. The spin-free-fixed frame is an extended one of a body-fixed frame, in which only z axis is fixed to the spin axis of the system.

The effect of the SRP on the sail membrane can be divided into specular reflection, diffuse reflection, and absorption. The force exerted on a microelement of the sail membrane by each effect is written as follows.[8)]

$$\begin{aligned} d\boldsymbol{f}_{spe} &= -2PC_{spe}(\boldsymbol{s}\cdot\boldsymbol{n})^2\boldsymbol{n}dS \\ d\boldsymbol{f}_{dif} &= -PC_{dif}\{(\boldsymbol{s}\cdot\boldsymbol{n})\boldsymbol{s} + B_f(\boldsymbol{s}\cdot\boldsymbol{n})\boldsymbol{n}\}dS \\ d\boldsymbol{f}_{abs} &= -PC_{abs}(\boldsymbol{s}\cdot\boldsymbol{n})\boldsymbol{s}dS \end{aligned} \tag{47}$$

Hence, the thrust and torque exerted on the spacecraft can be derived by the following equations.

$$\begin{aligned} \boldsymbol{F}_{SRP} &= \oint (d\boldsymbol{f}_{spe} + d\boldsymbol{f}_{dif} + d\boldsymbol{f}_{abs}) \\ \boldsymbol{T}_{SRP} &= \oint \boldsymbol{r}_M \times (d\boldsymbol{f}_{spe} + d\boldsymbol{f}_{dif} + d\boldsymbol{f}_{abs}) \end{aligned} \tag{48}$$

In order to the attitude and orbital motion properly, the thrust is described in the orbit-fixed frame and the torque is described in the spin-free-fixed frame.

In the actual way, only 2nd order static wave is used for the attitude control out of higher order ones. This is because the shape control accuracy deteriorates as the wave order increases. Replacing the superscript I in Eq. (45) with SF, the shape of the sail membrane in Σ^{SF} is expressed as follow.

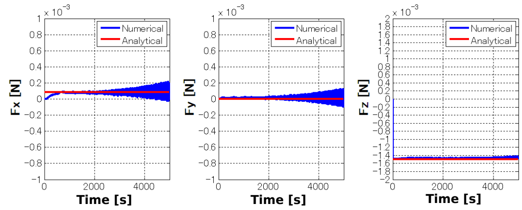

(a) History of force.

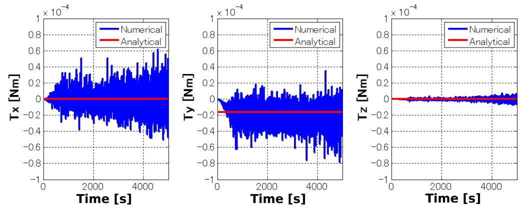

(b) History of torque.

Fig. 21.: Simulation results of force and torque on the sail membrane, obtained by the MPM.

$$w^{SF}(r,\theta) = w_1^{SF}(r,\theta) + w_2^{SF}(r,\theta) \tag{49}$$

Normal vector of the sail microelement can be derived by the following equation.

$$\boldsymbol{n} = \frac{\partial \boldsymbol{r}_M}{\partial r} \times \frac{\partial \boldsymbol{r}_M}{r\partial\theta} \tag{50}$$

From Eqs. (48), (49) and (50), the thrust and torque are expressed as follows, respectively.

$$\boldsymbol{F}^O_{SRP} = \begin{bmatrix} f_1(\psi,\phi) + f_2(\psi,\phi)\frac{\gamma_t A_1}{r_b}\cos a_1 + f_3(\psi,\phi)\frac{\gamma_t A_1}{r_b}\sin a_1 \\ f_4(\psi,\phi) + f_5(\psi,\phi)\frac{\gamma_t A_1}{r_b}\cos a_1 + f_6(\psi,\phi)\frac{\gamma_t A_1}{r_b}\sin a_1 \\ f_7(\psi,\phi) + f_8(\psi,\phi)\frac{\gamma_t A_1}{r_b}\cos a_1 + f_9(\psi,\phi)\frac{\gamma_t A_1}{r_b}\sin a_1 \end{bmatrix} \tag{51}$$

$$\boldsymbol{T}^{SF}_{SRP} = \begin{bmatrix} \tau_1\phi - \tau_2\frac{A_1}{r_b}\sin a_1 - \tau_3\frac{A_1A_2}{lr_b}\sin(a_2 - a_1) \\ \tau_1\psi + \tau_2\frac{A_1}{r_b}\cos a_1 + \tau_3\frac{A_1A_2}{lr_b}\cos(a_2 - a_1) \\ -\tau_4\frac{A_1}{r_b}(\psi\sin a_1 + \phi\cos a_1) \end{bmatrix} \tag{52}$$

where

$$\begin{aligned} \tau_1 &= (C_{dif} + C_{abs})PSl \\ \tau_2 &= \left\{\gamma_M(C_{dif} + C_{abs}) + (B_fC_{dif} + C_{spe})\right\}PSl \\ \tau_3 &= \frac{1}{2}\gamma_t(B_fC_{dif} + C_{spe})PSl \\ \tau_4 &= \gamma_M(C_{dif} + C_{abs})PSl \end{aligned} \tag{53}$$

$$\gamma_t = \frac{I_t}{I_t + I_M}, \quad \gamma_M = \frac{I_M}{I_t + I_M} \tag{54}$$

Formulations of $f_1(\psi,\phi)$ through $f_9(\psi,\phi)$ are written in Eq. (55). Thus, the thrust and torque can be controlled via A_1, A_2, a_1, and a_2.

In order to verify the validity of the analytical derivation of the thrust and torque, numerical simulation is conducted by the MPM. In addition to the evaluation of the shape control accuracy, which was conducted in section **4.3.**, the force and torque derive by SRP are calculated and output. Figure 21 shows one of simulation results. As can be seen from the figure, mean values of the numerical simulation correspond to the analytical values. Therefore, the formulations of the thrust and torque

$$
\begin{aligned}
f_1(\psi,\phi) &= -PS\,(2C_{spe}\sin\psi\cos^2\psi\cos^3\phi + B_f C_{dif}\sin\psi\cos\psi\cos^2\phi)\\
f_2(\psi,\phi) &= -PS\,(2C_{spe}\cos^2\psi\sin\phi\cos^2\phi + B_f C_{dif}\cos\psi\sin\phi\cos\phi)\\
f_3(\psi,\phi) &= -PS\,\{2C_{spe}\cos^3\psi\cos^3\phi + (C_{dif}+C_{abs})\cos\psi\cos\phi + B_f C_{dif}\cos^2\psi\cos^2\phi\}\\
f_4(\psi,\phi) &= PS\,\{2C_{spe}(\cos^3\psi\cos^2\phi - 2\sin^2\psi\cos\psi\cos^2\phi) + B_f C_{dif}(\sin^2\psi-\cos^2\psi)\cos\phi\}\\
f_5(\psi,\phi) &= -PS\,(6C_{spe}\sin\psi\cos^2\psi\sin\phi\cos^2\phi + 2B_f C_{dif}\sin\psi\cos\psi\sin\phi\cos\phi)\\
f_6(\psi,\phi) &= -PS\,(4C_{spe}\sin\psi\cos\psi\sin\phi\cos\phi + B_f C_{dif}\sin\psi\sin\phi)\\
f_7(\psi,\phi) &= PS\,\{2C_{spe}(\cos^2\psi\cos^3\phi - 2\cos^2\psi\sin^2\phi\cos\phi) - B_f C_{dif}\cos\psi(\sin^2\phi-\cos^2\phi)\}\\
f_8(\psi,\phi) &= -PS\,\{6C_{spe}\sin\psi\cos^2\psi\cos^2\phi + (C_{dif}+C_{abs})\sin\psi + 2B_f C_{dif}\sin\psi\cos\psi\cos\phi\}\\
f_9(\psi,\phi) &= -PS\,\{6C_{spe}\cos^3\psi\sin\phi\cos^2\phi + (C_{dif}+C_{abs})\cos\psi\sin\phi + 2B_f C_{dif}\cos^2\psi\sin\phi\cos\phi\}
\end{aligned}
\tag{55}
$$

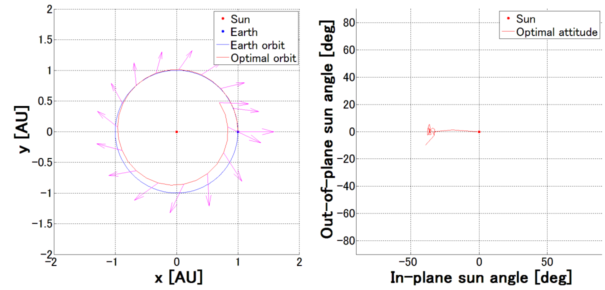

(a) Orbit history. Magenta arrows are thrust vectors caused by SRP.

(b) Orientation of the sail.

Fig. 22.: An example of the optimization problem of the attitude and orbit motion. The spacecraft is decelerated.

expressed in Eqs. (51) and (52), which is based on the simple theoretical model described in section **3.**, can be used to the attitude and orbit control of a spinning solar sail.

5.3. Optimization problem of attitude and orbital motion

As the summary of this study, an optimization problem of attitude and orbital motion of a spinning solar sail is solved. The analysis aims to achieve maximum acceleration/deceleration by utilizing the attitude and orbit control based on the shape control of the sail membrane. Initial position and velocity of the spacecraft are identical to those of Earth, and the initial attitude is the sun direction. For the simplicity, the orbital motion is limited in two dimensional one. The optimum control rule and the resulting attitude/orbital motion is calculated by a method called DCNLP (direct collocation with non-linear programming).[9] Control inputs are A_1, A_2, a_1, and a_2. Note that the propulsion performance (area / mass) of the solar sail used in this analysis is set to be better than that of IKAROS because the propulsion performance of IKAROS is not sufficient for the orbit control in realistic time span.

Figure 22 shows the optimization result of deceleration maneuver. Figure 22a confirms that the spacecraft is continuously decelerated. Figure 22b shows that the sail membrane keeps orienting toward a certain point. This point is the optimum direction to decelerate the spacecraft by photon propulsion. A noteworthy fact is that the orientation of the sail moves from the initial point to the optimum point almost linearly, despite the presence of disturbance. This owes to the small time constant of the 1st order static wave. The attitude control by the 2nd order static wave (i.e. canceling disturbance out) also works.

6. Conclusion

An active shape control method for a spinning membrane space structure is proposed. The applicability of the shape control method to the attitude and orbit control problem of a spinning solar sail is also presented. Deformation behavior of flexible structures such as membranes is so complex, and this study provides an effective solution to handle it. Use of flexible membrane structures in the space field is essential to the future space exploitation since they have many advantages to conventional space structures. The proposed shape control method gives an effective insight to the development of them.

In this study, the optimization problem of attitude and orbital motion is taken as one possible application of the shape control method. However, the method has various applicability to the deep space exploration missions.

References

1) Tsuda, Y., Mori, O., Funase, R., Sawada, H., Yamamoto, T., Saiki, T., Endo, T., and Kawaguchi, J.: Flight status of IKAROS deep space solar sail demonstrator, *Acta Astronautica*, **69** (2011), pp. 833-840.
2) Tsuda, Y., Saiki, T., Funase, R., and Mimasu, Y., "Generalized Attitude Model for Spinning Solar Sail Spacecraft," *Journal of Guidance, Control, and Dynamics*, **36** (2013), pp. 967-974.
3) Funase, R., Shirasawa, Y., Mimasu, Y., Mori, O., Tsuda, Y., Saiki, T. and Kawaguchi, J.: On-orbit verification of fuel-free attitude control system for spinning solar sail utilizing solar radiation pressure, *Advances in Space Research*, **48** (2011), pp. 1740-1746.
4) Nakano, T., Mori, O., and Kawaguchi, J.: Stability of Spinning Solar Sail-craft Containing a Huge Membrane, AIAA Guidance, Navigation and Control Conference and Exhibit, AIAA Paper 2005-6182, 2005.
5) Mori, O., Shirasawa, Y., Sawada, H., Tsuda, Y., Funase, R., Saiki, T., Yamamoto, T., Motooka, N., Jifuku, R.: Attitude Dynamics of Spinning Solar Sail "IKAROS" Considering Thruster Plume, *Trans. JSASS Aerospace Tech. Japan*, **10** (2012), pp. 27-32.
6) Shirasawa, Y., et al.: Analysis of Membrane Dynamics using Multi-Particle Model for Solar Sail Demonstrator "IKAROS", Proceeding of 52nd AIAA/ASME/ASCE/AHS/ASC Structures, Structural Dynamics and Materials Conference, Denver, 2011.
7) Chujo, T., Kawaguchi, J.: Evaluation of Transient Response of Spinning Solar Sail with Flexible Membrane by Eigenfunction Analysis and Continuum Analysis, *Acta Astronautica*, **127** (2016), pp. 542-552.
8) McInnes, C. R.: Solar Sailing: Technology, Dynamics and Mission Applications, Springer-Praxis, Chichester, UK, 1999.
9) Hargraves, C. R., Paris, S. W.: Direct Trajectory Optimization Using Nonlinear Programming and Collocation, *Journal of Guidance, Control, and Dynamics*, **10** (1987), pp. 338-342.